Rocking analysis of masonry walls interacting with roofs

Linda Giresini[1], Massimo Fragiacomo[2], Mauro Sassu[3]

[1]Department of Energy, Systems, Territory and Constructions Engineering
University of Pisa, l.giresini@unipi.it

[2]Department of Civil, Construction-Architecture & Environmental Engineering, University of L'Aquila, massimo.fragiacomo@univaq.it

[1]Department of Energy, Systems, Territory and Constructions Engineering
University of Pisa, m.sassu@unipi.it

ABSTRACT

This paper investigates the out-of-plane behavior of masonry walls interacting with roofs. Often, collapses of masonry portions supporting roof may occur due to the roof thrust, which generates a destabilizing effect over motion. Nevertheless, the roof weight can produce a positive stabilizing effect for rotation amplitudes smaller than the critical value. The dynamics of a rocking masonry block interacting with roof is discussed, by properly modifying the Housner equation of motion of the free-standing single degree-of-freedom block. The dependence of the restoring moment on the rotation angle is investigated and the minimum horizontal stiffness is calculated so that the same ultimate displacement as the system without roof thrust is obtained. Two case studies are presented as applicative examples of the proposed method: an URM structure tested on shaking table and a spandrel beam subjected to roof thrust that survived the Emilia Romagna earthquake. Inertia moments and radius vectors of different failure mechanisms are provided to solve the one-degree-of-freedom equation of motion for different block shapes. Finally a parametric analysis of a trapezoidal rocking block has been carried out by changing its geometrical shape. This analysis shows that the influence of the shape is relevant for the calculation of the failure load, although is not possible to determine an *a priori* most critical shape.

1 INTRODUCTION

Seismic vulnerability of unreinforced masonry (URM) buildings can be assessed by means of global and local analyses. However, connections between walls or between walls and floors are sometimes not efficient, making out-of-plane local analysis of wall panels regarded as rigid a more reliable tool to estimate their seismic performance [1,2]. Both limit equivalent static and dynamic analyses can be used. In the first one, a collapse multiplier is calculated by imposing a kinematic mechanism [3,4]; among all possible mechanisms, the lower bound theorem states that the minimum collapse multiplier provides a conservative estimation of the actual collapse load. Nevertheless, this method is not able to evaluate the evolution over time of motion, nor to take into account the dissipation properties of the system. By contrast, the

response of the rigid masonry block over time can be determined using dynamic analysis, in accordance with the fundamental observation that earthquakes can only be correctly described by acceleration time-histories [5]. Moreover, the so called "restitution coefficient", which considers the reduction in velocity after each impact of the rigid masonry block, can be properly used to describe the damping effect [6].

The current Italian code [7,8] prescribes the use of a kinematic, linear or non-linear, equivalent static analysis to verify the safety of these macro-elements. The kinematic analysis is based on the assumption that the overturning forces are statically applied with increasing intensity, in a synchronous way with the stabilizing force. From the principle of virtual work, simple relationships can be derived between the collapse multiplier and the rotation angle or the displacement of a significant point, such as the center of gravity or the top of the macro-element. This approach was found to be over-conservative [9] for the evaluation of the seismic vulnerability of rocking bodies, leading sometimes to the need to use potentially unnecessary consolidation techniques for the retrofit of historical buildings. For these structures the costs could be indeed high when installation of common tie-rods is not sufficient. Furthermore, retrofitting techniques resulting from over-conservative approaches can induce irreversible and invasive modifications to historic construction. For these reasons, a more respectful and prudential strategy is recommended in the application of preventive and reversible retrofitting techniques, as specifically suggested for historic churches [10,11] or historical walls near to collapse [12].The rocking analysis provides a more realistic approach for the dynamic behavior of rigid macro-elements, based on the solution of motions equations, for a given acceleration or displacement time-history and a proper damping value at the base, which modifies the velocity after each impact.
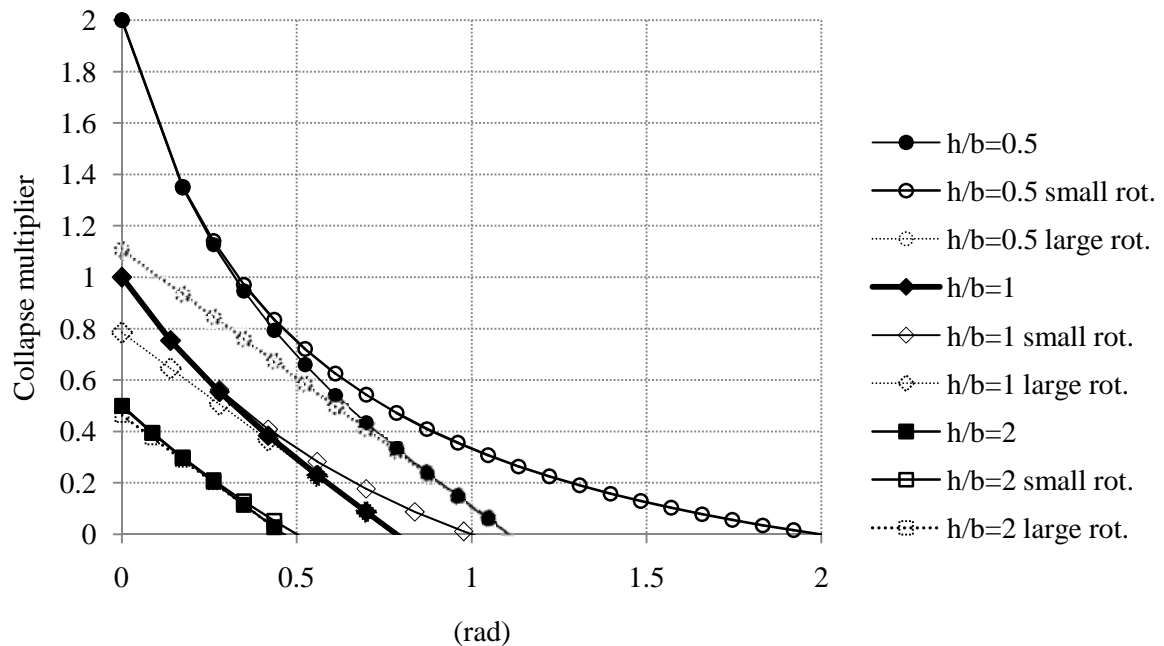
Fig. 1.Collapse multipliers of SDOF block with height 2h and base 2b (kinematic analysis). Solid marker: exact equation (Equation (1)); empty marker and solid line: small rotations (Equation (2)); empty marker and dotted line: large rotations (Equation (3)).

The collapse multiplier λ in the kinematic analysis of a single-degree-of-freedom (SDOF) rectangular block with height $2h$ and base $2b$ can be calculated by applying the principle of virtual work to a generic configuration of the block inclined by ϑ, obtaining:

$$\lambda = \frac{\frac{b}{h} - tan|\vartheta|}{1 + \frac{b}{h} tan|\vartheta|} = tan(\alpha - |\vartheta|). \tag{1}$$

The ultimate rotation equates to the slenderness ratio α, since the tangent function vanishes for $\alpha = |\vartheta|$.

If small rotations are considered, $tan\vartheta \cong \vartheta$: the less slender the block, the more over-conservative the collapse multipliers (Fig. 1):

$$\lambda = \frac{\frac{b}{h} - |\vartheta|}{1 + \frac{b}{h}|\vartheta|}. \tag{2}$$

Moreover, for large rotations, Equation (1) can be linearized to:

$$\lambda \cong \alpha - |\vartheta|, \tag{3}$$

valid for rotation values similar to the slenderness ratio α. In the latter equation the errors for the estimation of the collapse multiplier are larger for small rotations.
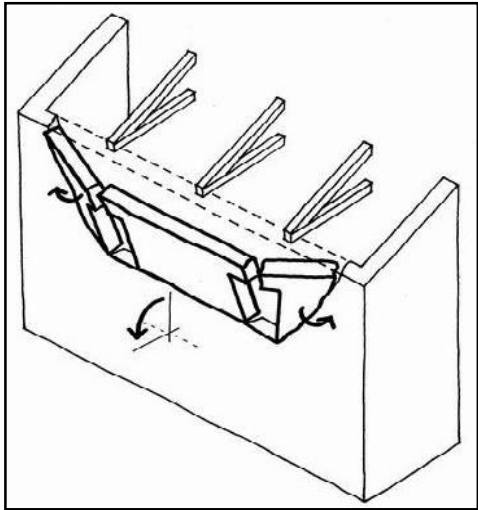
(a)

(b)

(c)

(d)

Fig. 2. Spandrel mechanisms interacting with timber roofs: (a) sketch of the typical mechanism (adapted from [13]), (b) photo of the spandrel mechanism in Reggiolo, Emilia Romagna 2012, (c) L'Aquila2009 and (d) Molise 2002.

Fig. 1 displays the collapse multiplier depending on the rotation angle ϑ for different h/b values, comparing the exact formula (Equation (1)) with the approximation for small rotations (Equation (2)) and with the formula for large rotations (Equation (3)). The difference between them becomes negligible for more slender blocks.

Existing masonry buildings are generally covered by timber roofs, frequently built with king-post trusses or beams, and completed by steel or wooden purlins and rafters. The effect of timber floors and roofs on masonry buildings subjected to local collapses relates to their weight and thrust applied to the top of the masonry panels. A relevant number of these damages (out-of-plane overturning of masonry blocks) was observed in the last Italian earthquakes (Umbria-Marche 1997, Molise 2002, L'Aquila 2009, Emilia Romagna 2012,Fig**. 2**). Rocking analysis can be useful for the interpretation of the corresponding failure mechanisms.

The rocking analysis is based on the classical Housner contribution [6]. The rocking problem was extensively analyzed in literature, by considering free-standing rigid blocks [14,15] or panels with horizontal [9] or vertical [16] restraints. Experimental tests on masonry walls were performed to support the theoretical background [17] and analyze the relevance of energy damping in the response [18]. The two previously mentioned methods, kinematic and rocking analysis, although based on the hypothesis of rigid blocks, are markedly different from each other: the former provides static relationships, while the latter follows the evolution of motion. It can be reasonably expected that the kinematic analysis is more conservative with respect to the rocking analysis. Nevertheless, sometimes this difference may be relevant, as it will be shown in the following paragraphs. Furthermore, if the kinematic analysis results are over-conservative, it will force structural designers to prescribe unnecessary retrofitting solutions, which could be not compatible with the historical character of the building.

2 DYNAMIC RESPONSE OF A SDOF BLOCK CONNECTED TO A ROOF

2.1 Equation of motion

The geometric parameters of the rocking block are the length of the semi-diagonal R of the block, which defines the block size, and the slenderness ratio α, given by the inverse of the tangent of the base to height ratio b/h, where $2b$ and $2h$ signify the thickness and the height of the block, respectively . The block is connected to a roof mass m_r, which is located at a distance d from the right corner (Fig.3a-Fig. 4a) and has a self-weight $m_r g$. When the roof is inclined with specific boundary conditions, as discussed later, a horizontal destabilizing thrust H_r may act, too.

Due to the eccentricity of the roof mass, the radius vector changes depending on the rotation sign, $R_{r.cw}$ for clockwise and $R_{r.cc}$ for counterclockwise rotations, respectively. In the integration of the motion equation, an event identification subroutine was set to identify the variable radius vector. However, for slender blocks the difference between $R_{r.cw}$ and $R_{r.cc}$ is negligible and the radius vector can be assumed as the double of the radius vector R. Let R_r be the current roof radius vector and the block be connected to a horizontal restraint. The analysis of this restrained configuration was performed in [9]. In that work, the Housner equation of motion was modified by adding a spring with axial stiffness K to represent an element with stabilizing effect, such as strengthening devices (tie-rods), transverse walls or flexible diaphragms. The stiffness K can have whatever value depending on the type of the

roof and on the type of the roof-wall connection. The equation describing the motion by neglecting the roof mass ($m_r = 0$) is:

$$I_0\ddot{\vartheta} + sgn(\vartheta)mgR\sin\hat{A} + sgn(\vartheta)KR_r^2\cos\hat{A}_r\ [sin\ \alpha_r - \ \sin\hat{A}_r] - m\ g\ddot{u}_gR\cos\hat{A} = 0, \qquad (4)$$

where $\hat{A} = \alpha - sgn(\vartheta)\vartheta$ and $\hat{A}_r = \alpha_r - sgn(\vartheta)\vartheta$.

where m is the block mass and $\ddot{u}_g$ is the acceleration time-history (in gravity acceleration g units) of the mass. I_0 is the polar inertia moment with respect to the base corner O, $I_0 = \frac{4}{3}mR^2$.

(a)   (b)
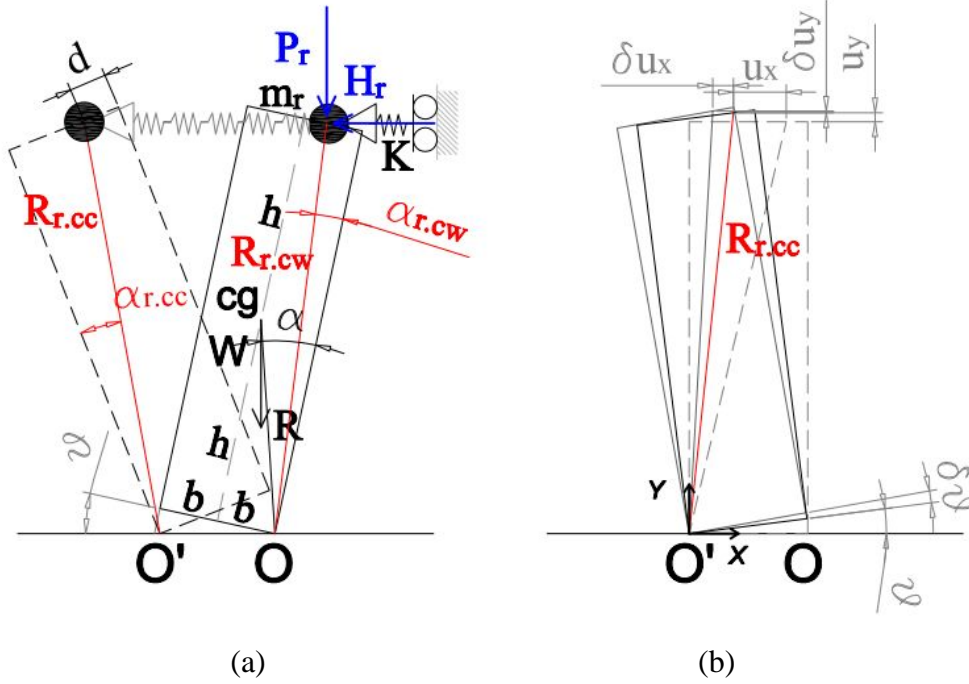
Fig. 3. The rocking block with horizontal elastic restraint and roof mass (a);virtual horizontal and vertical displacements of the roof center of mass (b).

To include the dependence on the roof weight in the equation of motion, the differential displacement δu_y of its application point has to be calculated (Fig. 3b). By starting from a deformed configuration (initial rotation angle equal to ϑ), an infinitesimal rotation $\delta\vartheta$ determines the vertical displacementδu_y as:

$$\delta u_y = R_r\sin\hat{A}\ \sin\delta\vartheta. \qquad (5)$$

The virtual work done by the roof weight is expressed as:

$$\delta W = \frac{\partial W}{\partial\vartheta}\delta\vartheta = P_r\delta u_y = -sgn(\vartheta)\ m_rgR_r\ \sin\hat{A}\sin\delta\vartheta \qquad (6)$$

Assuming that the linearization of the trigonometric term depends on the virtual rotation angle, the derivative of the work W with respect to ϑ is given by:

$$\frac{\partial W}{\partial\vartheta} = -sgn(\vartheta)m_rgR_r\ \sin\hat{A} \qquad (7)$$

the opposite of which gives the potential energy to be added in the Euler-Lagrange equation, leading to:

$$I_{0c}\ddot{\vartheta} + sgn(\vartheta)\,mgR\sin\hat{A} + sgn(\vartheta)KR_r^2\cos\hat{A}_r\,[\sin\alpha_r - \sin\hat{A}_r] + \qquad (8)$$
$$+ sgn(\vartheta)\,m_r g R_r \sin\hat{A}_r - (mR\,\cos\hat{A} + m_r R_r\cos\hat{A}_r)\,\ddot{u}_g g = 0$$

where the polar moment I_{0c} includes the roof mass contribution by increasing the radius vector of the block to account for the effect of the roof mass, which leads to a higher centroid position [19]. Indeed, the roof mass is assumed to participate to the rocking motion by rotating together with the masonry block. In the case of no eccentricity (Fig. 4b), the distance of the centroid of the composed system G_c is:

$$h_{G_c} = \frac{(m + 2m_r)h}{m + m_r} \qquad (9)$$

and the inertia moment of the system is obtained by calculating it first with respect to G_c and then with respect to O (or O'):

$$I_{0c} = \frac{4}{3}mR^2 + m_r R_r{}^2. \qquad (10)$$

(a)   (b)
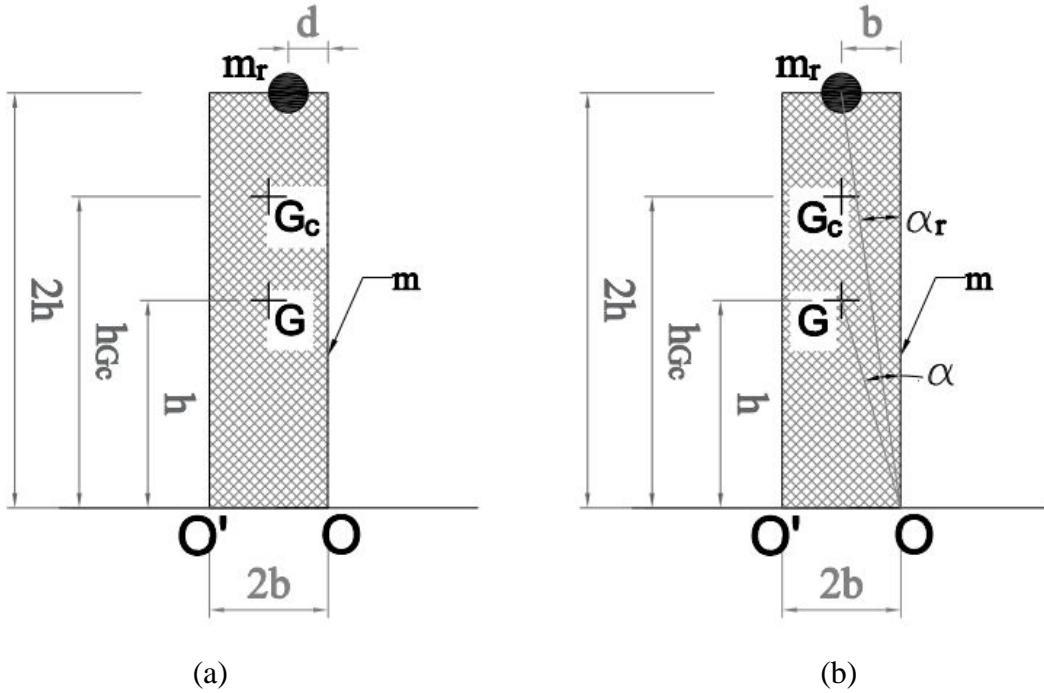
Fig. 4. Centroid of the composed masonry block + roof mass system : with (a) and without (b) eccentricity.

The inertial effect of the mass at the top of the block is considered in Equation (8) in the excitation term depending on $\ddot{u}_g$. The acceleration applied to the added mass is assumed the same as that applied to the center of gravity of the block itself.

Similarly, the horizontal differential displacement δu caused by the roof thrust is given by:

$$\delta u_x = R_r \cos\hat{A} \, \sin\delta\vartheta \qquad (11)$$

By following the same procedure of Equation(6) to (9), the equation of motion of a block horizontally restrained and subjected to additional mass and horizontal thrust is:

$$I_{0c}\ddot{\vartheta} + sgn(\vartheta)\,mgR\sin\hat{A} + sgn(\vartheta)KR_r^2\cos\hat{A}_r\,[\sin\alpha_r - \sin\hat{A}_r] +$$
$$+sgn(\vartheta)\,m_r gR_r\sin\hat{A}_r - H_r R_r\cos\hat{A}_r - (mR\cos\hat{A} + m_r R_r\cos\hat{A}_r)\,\ddot{u}_g g = 0 \qquad (12)$$

The direction and magnitude of the vector H_r can be assumed constant during motion in the hypothesis of small displacements. In this paper, damping effects are taken into account in the Housner's formulation using the theoretical value of the restitution coefficient e valid for rectangular blocks [6]:

$$e = 1 - \frac{3}{2}\sin^2\alpha. \qquad (13)$$

3   EFFECT OF THE ROOF THRUST AND HORIZONTAL RESTRAINT

The effect of the roof thrust and horizontal restraint on the restoring moment is analyzed from a static perspective. The restoring moment of the system with additional mass m_r, no roof stiffness ($K = 0$) and no roof thrust ($H_r = 0$) is drawn in Fig. 5 with a solid line. Let the roof mass be placed without eccentricity (Fig. 4b), with radius vector R_r. Thus:

$$M_r(\vartheta) = mgR\sin(\alpha - \vartheta) + m_r gR_r\sin(\alpha_r - \vartheta) \qquad (14)$$

By imposing the condition $M_r(\vartheta_u) = 0$ one obtains:

$$\tan\vartheta_u = \frac{mR\sin\alpha + m_r R_r\sin\alpha_r}{mR\cos\alpha + m_r R_r\cos\alpha_r} \qquad (15)$$

If, as it is usually the case for masonry walls, $m_r \ll m$, the maximum ϑ value (ϑ_u) can be assumed equal to the slenderness ratio α (Equation (1)) as the additional mass becomes negligible.

The expression of the restoring moment $M_r(\vartheta)$ with $K = 0$ and a horizontal thrust H_r is, for $\vartheta(t) > 0$:

$$M_r(\vartheta) = mgR\sin(\alpha - \vartheta) + m_r gR_r\sin(\alpha_r - \vartheta) - H_r R_r\cos(\alpha_r - \vartheta) \qquad (16)$$

The dashed line in Fig. 5 displays the restoring moment depending on the rotation when a roof thrust H_r is applied. For $\vartheta = 0$, the acceleration that triggers motion is decreased by the quantity $H_r R_r\cos\hat{A}_r$ with respect to the initial configuration. Due to the destabilizing effect of the thrust, the ultimate rotation corresponding to a null restoring moment is lower than α:

$$\tan\vartheta_{u,H_r} = \frac{mgR\sin\alpha + m_r gR_r\sin\alpha_r - H_r R_r\cos\alpha_r}{mgR\cos\alpha + m_r gR_r\cos\alpha_r + H_r R_r\sin\alpha_r}. \qquad (17)$$

By adding a horizontal spring with axial stiffness K, which takes into account the roof flexibility, one has:

$$M_r(\vartheta) = mgR\sin(\alpha - \vartheta) + m_r gR_r\sin(\alpha_r - \vartheta)$$
$$- H_r R_r\cos(\alpha_r - \vartheta) + KR_r^2\cos(\alpha_r - \vartheta)\,[\sin\alpha_r - \sin(\alpha_r - \vartheta)]. \qquad (18)$$

7

To obtain the same displacement capacity of the system without thrust, it is possible to calculate the minimum stiffness K_{min} for which the rotation capacity increases to ϑ_u (dashed-dotted line in Fig. 5), by imposing the condition $M_r(\vartheta) = 0$ in Equation (16) and $\vartheta = \vartheta_u$ in Equation (18):

$$K_{min} \cong \frac{H_r}{R_r} \frac{1}{[\sin \alpha_r - \sin (\alpha_r - \vartheta_u)]},\tag{19}$$

since the first two terms of $M_r(\vartheta)$ vanish and the term $\cos(\alpha_r - \vartheta)$ is simplified. If the additional mass is negligible (namely, $\vartheta_u \cong \alpha$) and it is applied at the top of the panel, namely $\alpha \cong 2\alpha_r$, the minimum stiffness value is:

$$K_{min} = \frac{H_r}{R_r} \frac{1}{2\sin \alpha_r},\tag{20}$$

The larger the additional mass with respect to the block mass, the more this equation underestimates the value of K_{min}. Equation (20) is displayed in Fig. 6.
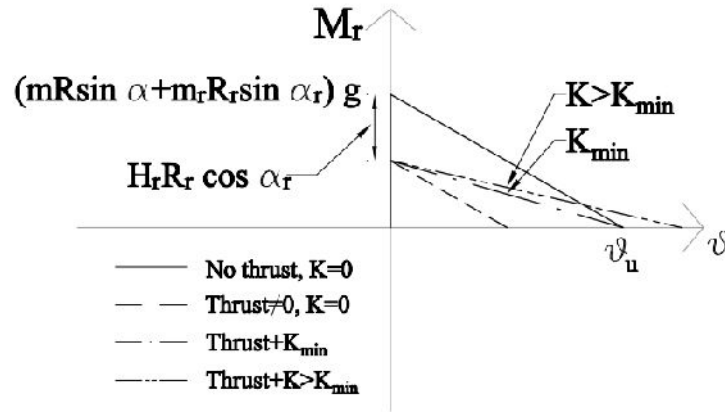
Fig. 5.Moment-rotation relationships with and without thrust and horizontal stiffness K.

This stiffness value represents a minimum, depending on the thrust and the spring position, for which the negative effect of the outward thrust is vanished. Stiffness values $K > K_{min}$ reduce the softening of the system (double dotted line in Fig. 5). The minimum stiffness K_{min} tends to zero for squat blocks (when $\alpha > 0.3$ rad) and a scale effect is observed: larger blocks require a lower minimum stiffness to obtain the same ultimate displacement as the system without thrust.

4 ROCKING MASONRY WALL CONNECTED TO A HORIZONTAL TIMBER ROOF

A numerical program was written to solve Equation (12). The program was implemented in MATLAB *R2013* adopting the ODE45 solver, which uses the 4th-5th order Runge-Kutta integration technique [20]. As a first example, a case study of a two-storey masonry building with timber roofs part of the TREMA experimental test [21,22] has been considered.

4.1 Geometrical and mechanical properties of the case study building

The masonry building investigated is the 1st prototype (unreinforced version) built at the CNR-ENEA research centre of Casaccia, Rome (Italy). The URM building was tested to collapse on shaking table. The applied seismic record was the acceleration time-history recorded in Colfiorito (Perugia, Italy) during the Umbria-Marche earthquake of September 26th, 1997 (6.1 Richter magnitude, epicenter in Annifo-Colfiorito).
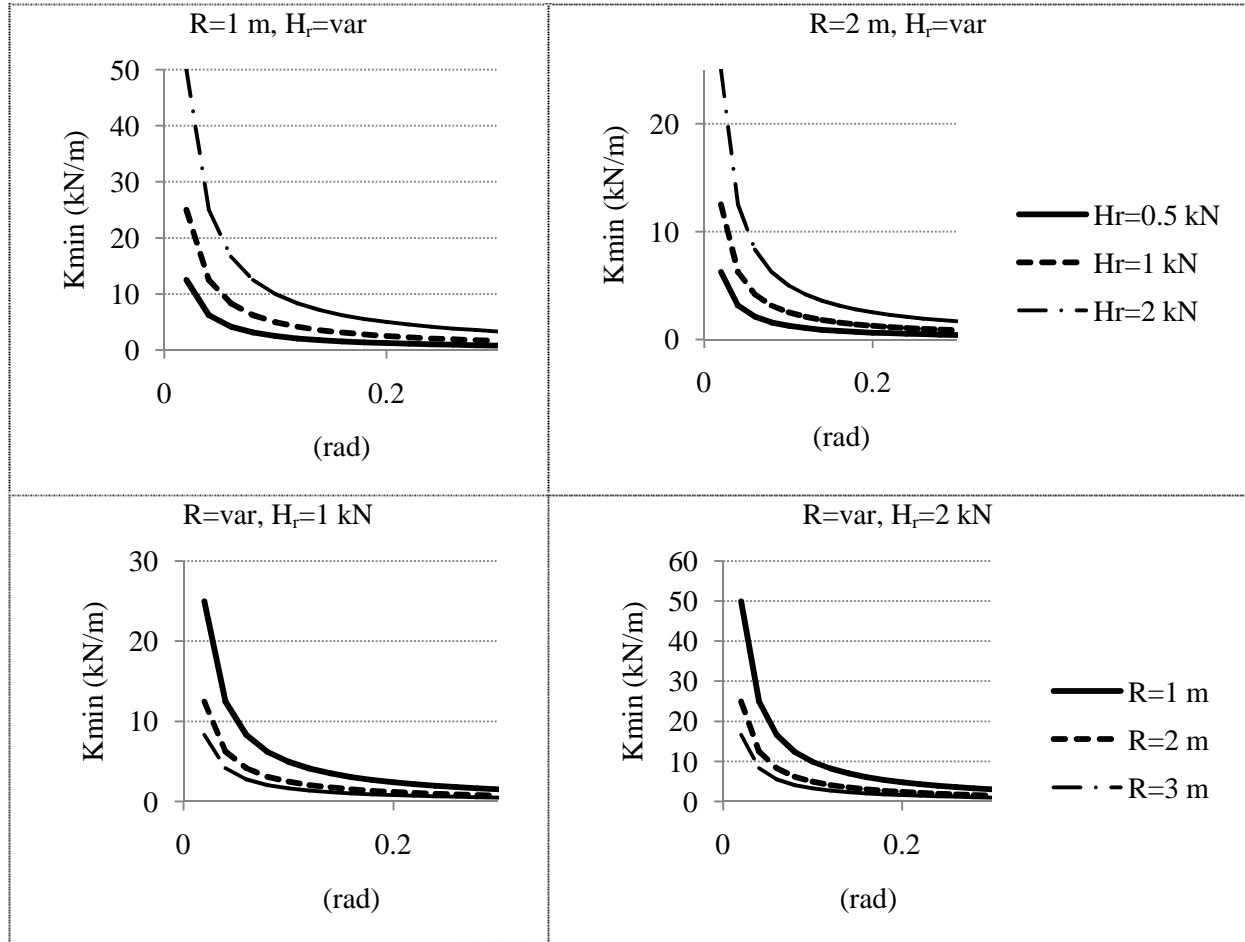
Fig. 6. Minimum stiffness value K_{min} leading to the same ultimate displacement of the masonry block without thrust (spring located at the top of the block with no eccentricity, Equation (20)).

The North-South and West-East components were simultaneously applied during the test. To take into account the scaled geometry - 1:1.5 - of the prototype, the seismic record was scaled by a factor equal to the square root of the adopted geometric scale. The building was constructed with rubble masonry made by calcareous tuff stone and lime-cement mortar, with a single room of 3.0×3.5 m^2 dimensions and interstorey height 2.15-2.20 m (Fig. 7). The 250 mm thick walls supported timber joists of 100×180 mm^2 cross section. Timber boards 20 mm thick were connected with nails to the five timber joists on each floor. The joists were simply supported on the masonry panels, and could therefore slide on them once the friction is overcome. The total weight of the masonry elements was about 169.71 kN. The prototype was constructed over a reinforced concrete (RC) base with a depth of 0.40 m and a weight of 28.25 kN. To fulfil the similitude scaling laws, a distributed mass of 2.5 t was placed on each floor [23].
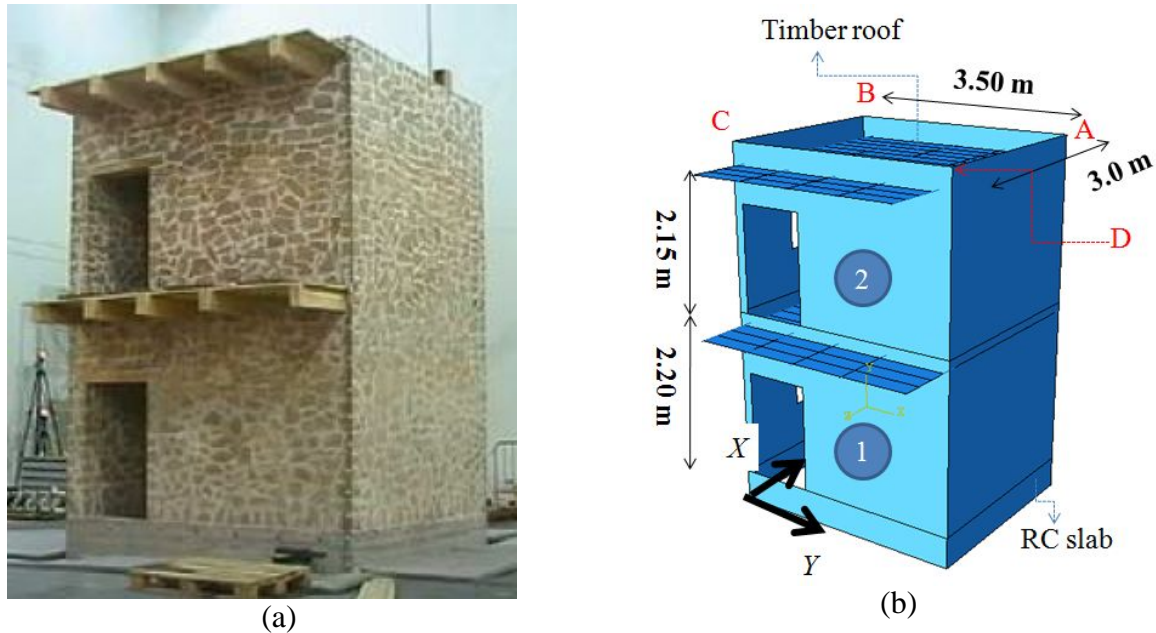
Fig. 7. Photo of the TREMA building (unreinforced version) tested on shaking table at ENEA Casaccia (a) and 3D drawing of the prototype with dimensions (b)

4.2 Experimental test results

An incremental dynamic analysis was performed by increasing the PGA value from 0.05g to 0.50g with nine steps of 0.05g each [22]. Up to 0.10g, no damage was observed. At 0.15g, a 10mm-gap vertical crack formed between AD and CD walls (Fig. 7b). The crack becomes larger at 0.25g, when it extended to the first storey from the top (panel 2 in Fig. 7b). At 0.3g significant out-of-plane displacements occurred, identifying a clear rocking phenomenon; at 0.40g the failure of the corners of panel 2 was attained and, at 0.45g, the collapse of the spandrel above the opening occurred (Fig. 8). Finally, at 0.50g the full collapse of the panel 2took place. Probably, the rocking of the façade started at about 0.25g, eased by the sliding of timber roof and by the crack formation in the corners C and D.


Fig. 8. The TREMA building at 0.45*g*: rocking of the upper wall

10

4.3 Rocking analysis

The overturning mechanism of the upper panel of façade CD (Fig. 7b) was considered. Based on the results of the experimental test, indeed, the crack at corners C and D formed at the first level [22].

Three conditions for the façade have been considered: (i) free-standing block, (ii) block restrained by a horizontal spring with stiffness K (Equation 8) and (iii) block subjected to the rebound effect due to one-sided oscillation[24]. The latter analysis allows the user to simulate the rebound effect caused by transverse walls by changing the sign of the velocity after the impact and by multiplying it by a damping and the restitution coefficient. An average damping coefficient of 0.9 was assumed in the analyses. Case (ii) entails the choice of an equivalent stiffness value for the timber floor. The stiffness value $K=357159$ N/m was adopted for a floor made of a single panel sheathing as suggested by the FEMA 356 [25].The stiffness plays a role only in one direction, in accordance with what discussed in [9], namely for negative rotations.

(a)

(b)

(c)
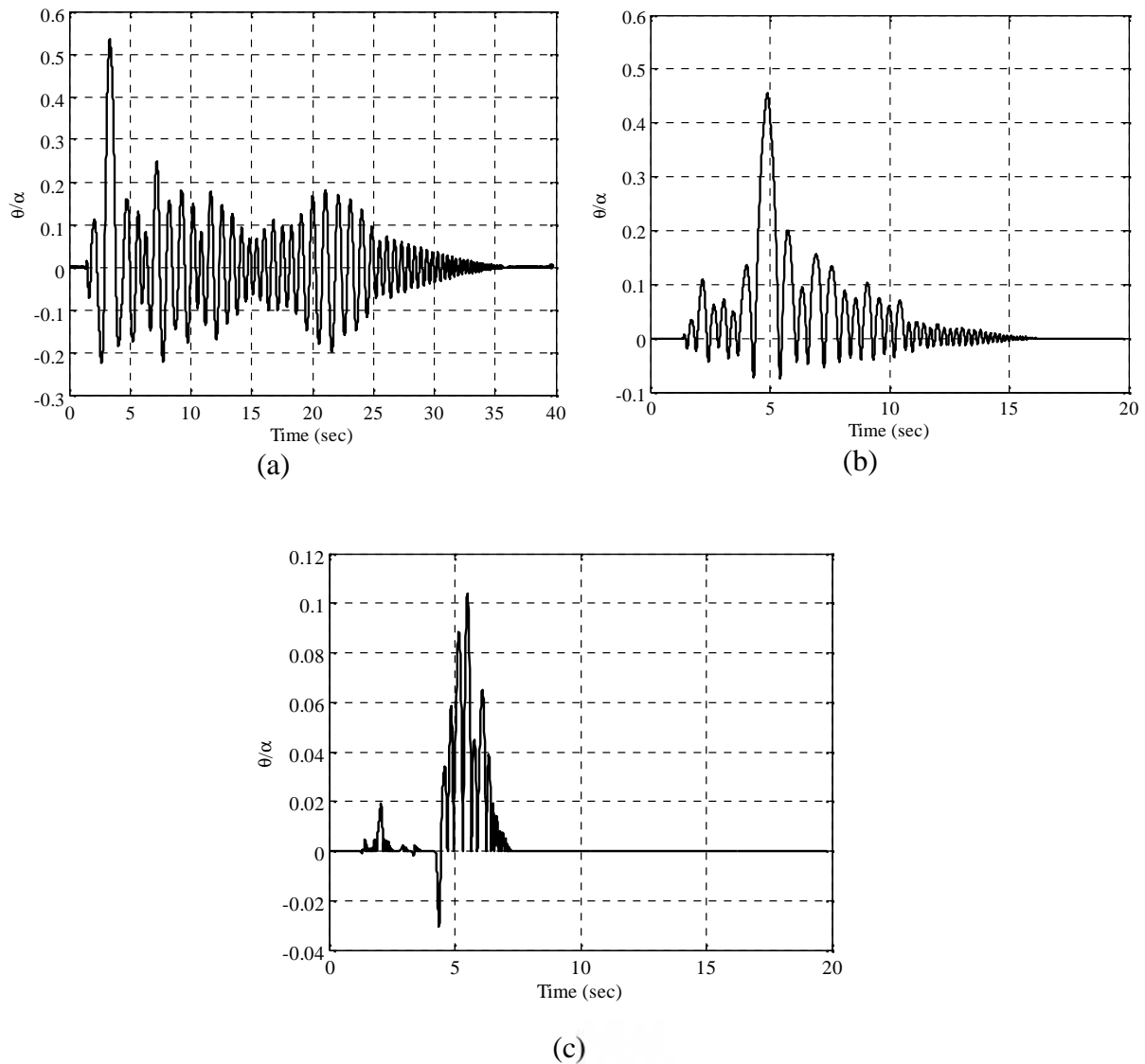
Fig. 9.Rocking analysis results (PGA=0.3g) for the upper façade mechanism: free-standing block (a); restrained façade with roof stiffness $K=357159$ N/m (b); rebound effect given by external walls, $r_f=0.9$ (c).

Moreover, no thrust is applied since the roof is horizontal. The free-field seismic record of Colfiorito was applied with incremental steps, starting from a PGA=0.05g and increasing it accordingly to what was done in the experimental test. The East-West direction of the earthquake corresponds to the X direction displayed in Fig. 7b. Since the acceleration demand increases when the failure mechanism does not occur on the ground, the acceleration that activates motion should be amplified by a factor AF given by the Italian regulations [7] for secondary and non-structural elements:

$$AF = \frac{3\left(1+\frac{Z}{H}\right)}{1+\left(1-\frac{T_a}{T_1}\right)^2} - 0.5 \tag{21}$$

where Z is the height of the rocking block base above the ground level, H the whole building height, while $\frac{T_a}{T_1}$ is the ratio of the rocking block vibration period to the whole building vibration period in the considered direction, in this case 11.93. The vibration period of the rocking block $T_1 = 0.11$ s is obtained from the kinematic analysis [8] whereas the building period is $T_a = 1.32$ s [23]. Since for the case under study the application of Equation (21) would result in a negative amplification factor, an unscaled (AF=1) seismic record was applied to the structure.

In rocking, overturning condition is assumed for a rotation of /2, therefore the normalized maximum rotation ϑ/α is about 13.6. Fig. 9 shows the response related to the case of PGA=0.3g, for which the block has just begun rocking motions. The cases with restraints are less severe than the free-standing case, anyway the block easily survives the excitation, since the maximum normalized rotation attains about 0.55. However, it is interesting to notice that with the formulation with timber diaphragm (Fig.9b) is less conservative than that where the rebound effect is considered (Fig.9c). In order to take into account the worst case, only the free-standing block is considered in the following.

(a) (b)
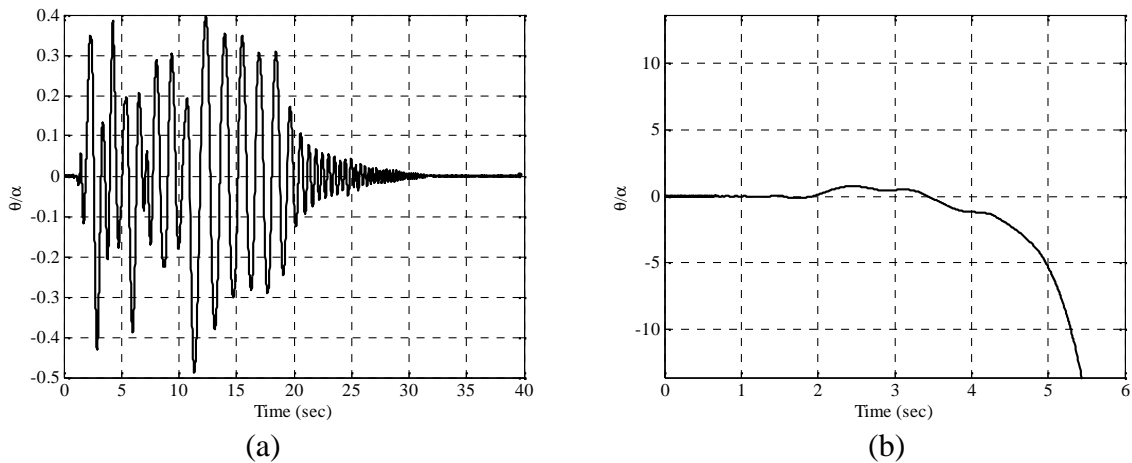
Fig. 10.Block response when PGA=0.5g (a) and collapse for PGA=0.51g (b) (upper façade mechanism)

It is interesting to notice that, for a PGA=0.5 g, the block survives (Fig. 10a), but it is sufficient to slightly increase the PGA to 0.51 g to attain collapse (Fig. 10b). This unstable situation was already found in literature for cosine-pulse type excitation [26,27]. This PGA value is exactly the collapse value, hence confirming the results of the shaking table test.

12

The safety verification was also carried out according to the non linear kinematic approach prescribed by the Italian code [5, 7]. This procedure is based on calculating the ultimate displacement as the displacement of the center of gravity corresponding to a collapse multiplier equal to zero. The ultimate displacement has to be compared with a demand displacement $S_{De}(T_s)$ obtained from a displacement spectrum at the secant period, taken as 0.16 times the ultimate displacement. The mechanism is unsafe when the ultimate displacement is lower than the demand one. The mechanism is predicted to occur for PGA=0.25 g (Table 1). The kinematic analysis markedly underestimates the actual collapse PGA of 0.50 g. The kinematic approach is therefore overly conservative for the considered record, which might not be acceptable for historic or strategic buildings, where possible retrofitting measures could induce unjustified alterations of the original constructive features. However, it must be pointed out that a single case is not representative of a general trend and a wider analysis involving other seismic records should be performed to draw final conclusions.

Table 1
Kinematic non-linear analysis (* indicates unsatisfied safety verification according to the kinematic analysis, the last row indicates the maximum PGA according to incremental non linear dynamic analysis) for the upper façade mechanism.

$S_{De}(T_s)$ [cm]	PGA (g)
3.20	0.10
4.82	0.15
6.40	0.20
8.01	**0.25***
9.60	0.30
11.23	0.35
12.84	0.40
14.44	0.45
16.02	0.50

5   SPANDREL BEAM CONNECTED TO A HIP-ROOF

The rocking analysis has been carried out also for the failure mechanism involving the spandrel beam below a timber roof, case very frequent in masonry buildings. The outer thrust of the roof could cause the overturning of the spandrel above the opening (Fig. 12). The inertial effects of the masonry self-weight and of the roof stabilize the block, which can be regarded as rigid.

In this case, the masonry is made by bricks and clay mortar, with specific weight 18 kN/m³. The spandrel beam depth is 1.50 m, the equivalent thickness 0.40 m with length variable from 0.80 m to 3.30 m. The spandrel beam weight is 22.2 kN. The inclination of the roof is 18°; the timber roof applies to the spandrel beam a vertical load of 4.98 kN and a thrust of 1.15 kN. The block survived the seismic input recorded in Moglia, a seismic station nearby with the same soil type C (Fig. 12a). From Equation (21), an amplification factor *AF*=1.04 is calculated, being $\frac{T_a}{T_1}$=2.68 and the ratio *Z/H*=0.96. The response displayed in Fig. 12 has been obtained by applying *AF* to the real seismic record; with this assumption, no collapse is predicted.
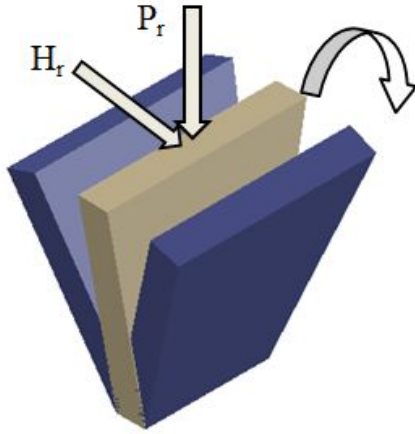
(a)

(b)

Fig. 11.Rocking mechanism of a spandrel beam subjected to roof weight and thrust (a) and case study building (Reggiolo, Emilia Romagna 2012)(b). H_r, horizontal thrust; P_r, vertical weight.

By contrast, the element is unsafe when a kinematic non-linear analysis is performed: the maximum demand displacement, referred to Moglia and equal to $S_{De}(T_s = 0.87\ s) = 6.88$ cm, is higher than the capacity, of 6.74 cm. Consequently, the Italian code approach is again conservative with respect to the rocking analysis results. However, the kinematic analysis is a useful tool to calculate the acceleration PGA_0 that initiates rocking. In this case $PGA_0 = 0.128$ g is lower than the maximum PGA of 0.236 g for the Moglia earthquake (by neglecting a possible amplification due to the position of the block).
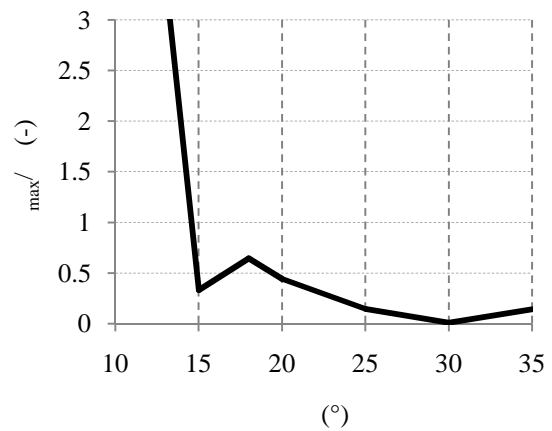
A parametric analysis, where the roof inclination ψ is varied, is carried out to investigate the effect of the outward thrust. The thrust depends on the roof inclination according the following equation:

$$H_r = \frac{p_r L}{4\ tan\ \psi} \tag{22}$$

where p_r is the uniformly distributed vertical load and L the total length of the symmetrically inclined roof loading the spandrel.
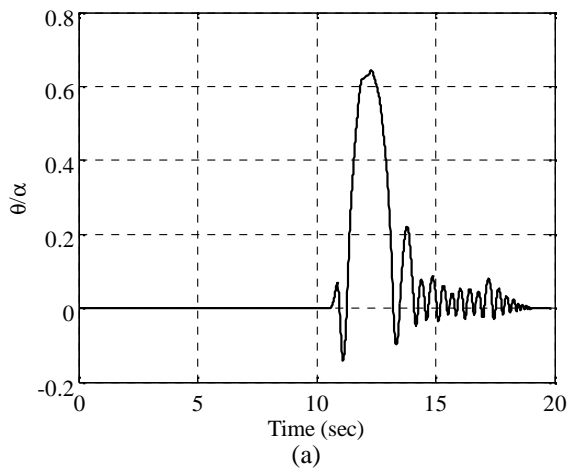
(a)

(b)

Fig. 12. Rocking spandrel beam response to Moglia (MOG) seismic record, North-South component (amplification factor =1.04) (a); normalized rotation depending on the roof inclination ψ (b).

14

Fig. 12b displays the maximum normalized amplitude ratio ϑ_{max}/α under Moglia seismic record with the roof weight considered as constant. For a roof inclination between 10° and 15°, the block suddenly collapses due to the high thrust. It is worth noting that between 20° and 35° the presence of the thrust does not significantly affect the maximum amplitude value. Conversely, between 10° and 15° there is a sudden collapse (the collapse is considered attained for a rotation value of /2 or ϑ_{max}/α=8.05); consequently, it is recommended that the thrust roof is conservatively considered with a properly reduced inclination - say by 20%. This takes into account possible uncertainties in defining the correct inclination and the corresponding roof thrust value. However, it is necessary to notice that not all inclined roofs generate a thrust on the bearing walls, as it depends on the boundary conditions of the roof. For this reason, it could be over-conservative to always apply a thrust when the roof is inclined.

6 PARAMETRIC ANALYSIS FOR DIFFERENT BLOCK GEOMETRY

6.1 Seismic records and assumptions

The response of a trapezoidal block was analyzed when its geometry varies with the angles and . Appendix A contains the formulas of the moment of inertia and radius vector of the trapezoidal block and of the corner mechanism. If the collapse mechanism is known in advance, for instance after an earthquake, the values of and are defined. Nevertheless, when it is necessary to perform a vulnerability assessment of an existing masonry building and no information is available about the shape of the rocking block, the structural designer should verify the response for different values of the angles and . The aim of this paragraph is to investigate the dynamic response of a trapezoidal block with fixed base of 1.0 m and height of 2.0 m, and variable angle under four recorded earthquake ground motions (Table 2). The seismic records have been chosen with PGV (peak ground velocity) in the range 25 to 45 cm/s. Furthermore, a high intensity earthquake ground motion with PGV>100 cm/s (Cape Mendocino) has been considered to investigate the effect of high intensity ground motions on the structural response.

The analysis has been carried out by considering 0.16 m and 0.20 m (cases #1-2 in Table 3) thick free-standing masonry blocks. In addition, for the wall thickness of 0.20 m, the effect of the roof has been taken into account: in case #3, the uniformly distributed loads on the roof of p_r=200 N/m (3) and 400 N/m (4) have been added, corresponding to an additional mass respectively of 1/36 and 1/18 of the masonry panel mass. In case #4, a distributed outward thrust of 50 or100 N/m has also been applied in addition to the roof distributed weights (Table 3). By varying the angle , the resultant additional weights and horizontal actions vary as well. The inertia moment of the system composed by the trapezoidal block and the additional mass, if any, is obtained similarly to Equation (10) using the formula:

$$I_{0c} = I_{0,XX,tr} - m_{tr}R_{tr}{}^2 + m_{tr}\left(h_{G_c} - h_{tr}\right)^2 + m_r\left(h - h_{G_c}\right)^2 + (m + m_r)\left(h_{G_c}{}^2 + s^2\right) \qquad (23)$$

where $(I_{0,XX,tr} - m_{tr}R_{tr}{}^2)$ is the inertia polar moment of the trapezoidal block with respect to its centroid, m_{tr} and m_r signify the block mass and the additional roof mass respectively, h_{G_c} denotes the distance from the base of the centroid of the block + mass system . The other symbols are indicated in Fig. (13). The highest and lowest values of inertia moment reported in Table 3 are obtained for $\beta = 0$ and $\beta = 1$ respectively.

Eventname	Date	MW	Station	Soiltype (Eurocode)	Component	PGA (g)	Network	Depth (km)	PGV (cm/s)	Repi (km)
MOG	05-29-2012	6.0	Moglia	C	E-W	0.236	I	10.2	26.61	16.4
FRIULI	09-11-1976	6.0	Gemona	B	E-W	0.236	I	4.3	36.68	9.4
AQV	06-04-2009	6.3	L'Aquila-V Aterno	B	E-W	0.657	I	8.3	42.0	5.1
CAPEMEND	04-25-1992	7.1	Cape Mendocino	-	0	1.346	U	9.6	127.4	10.4

Table 3
Cases investigated in the parametric analysis, $0 \leq \beta \leq 1$.

| Case #	2b (m)	I_{0c} (Nms^2)	Distributed weight p_r at the top of the block (N/m)	Horizontal thrust H_r at the top of the block (N/m)
1	0.16	788 I_0 4461	0	0
2	0.20	988 I_0 5591	0	0
3a	0.20	1070 I_0 6182	200	0
3b	0.20	1070 I_0 6182	200	50
4a	0.20	1152 I_0 6773	400	0
4b	0.20	1152 I_0 6773	400	50

The parameter varies in the range from 0 rad to 1 rad (=0-0.2-0.4-0.6-0.8-1.0). In this way, different block shapes can be considered since the collapse mechanism is not known in advance. An incremental dynamic analysis is performed for a symmetric block shape, namely = , by scaling the natural seismic records by a reduction factor (labeled RF) of 0.5. The reason for the choice of this reduction factor is the large number of collapses that occur in rocking analysis without scaling the original seismic records, which would prevent a critical analysis of the influence of the additional mass and of the outward horizontal thrust.

Fig. 13. Parametric analysis of a trapezoidal shape symmetric block with variable .

6.2 Rocking analysis

A selection of results of the rocking analysis is displayed in Fig. 14. The graphs show the value of maximum normalized amplitude ratio ϑ_{max}/α depending upon the angle . Where the curves of the cases specified in the legend are not displayed, it means that collapse occurs for all values. In addition, the vertical lines signify that the collapse occurs for values lower or larger than the corresponding value (for instance, in Fig. 14a collapse occurs when $0.0< <0.8$).
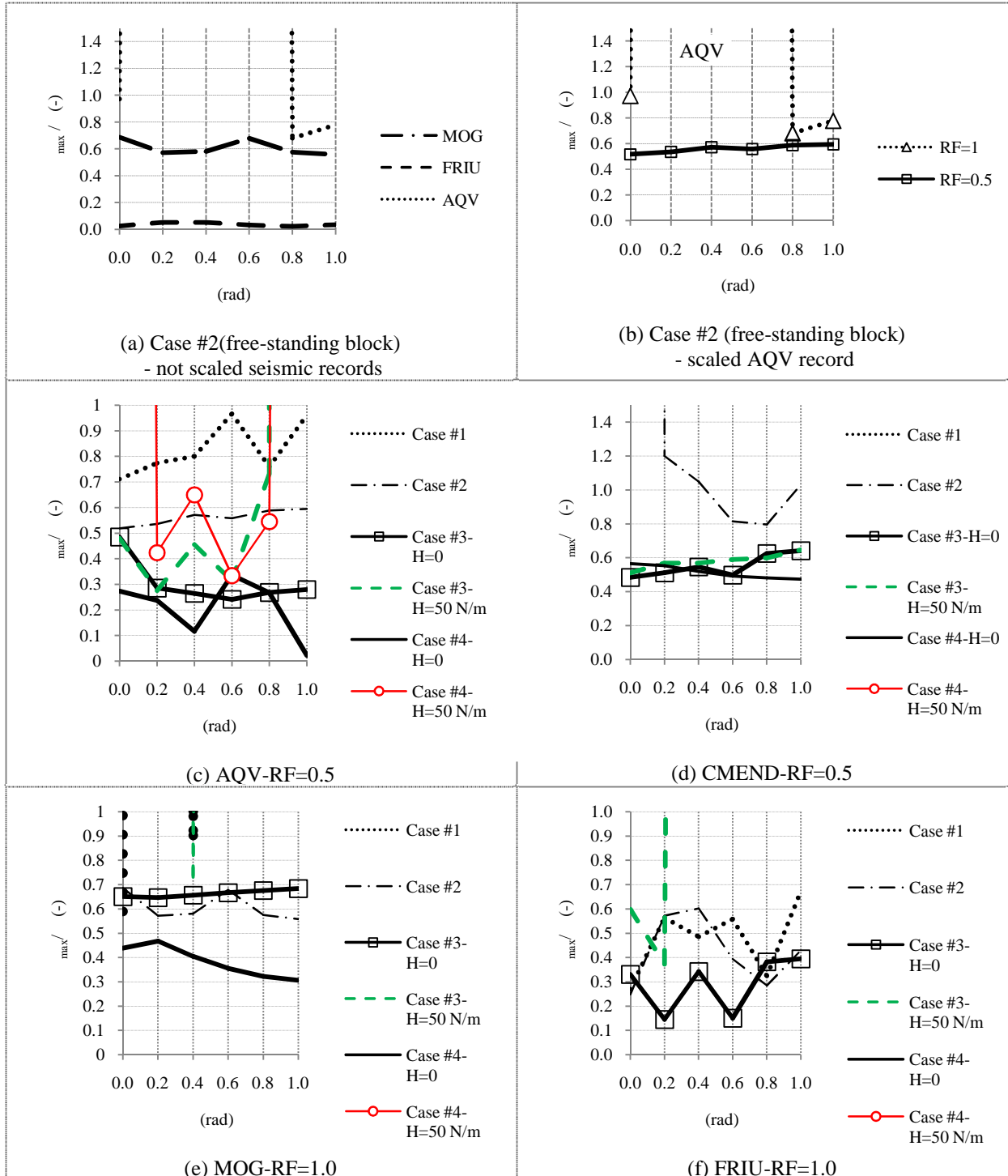
Fig. 14. Results of the parametric rocking analysis (RF, reduction factor; MOG, Moglia; FRIU, Friuli; AQV, L'Aquila; CMEND, Cape Mendocino)

17

As general comment, the larger , the lower α, the higher R. That means that, for the scale effect of the block size, larger values lead to more stable blocks, but a higher slenderness could result in a worse stability condition. Therefore, it cannot be stated *a priori* that the block is safer when is larger or viceversa. First it can be noticed that, in most cases, the response is markedly dependent upon the considered seismic record by varying the block shape (variable). By comparing the responses to Moglia and L'Aquila records, it can be seen that there is not a monotonic response with . In other words, larger , namely larger mass and rotational inertia, does not necessarily imply a more stable block (Moglia in Fig. 14a). One of the incremental analysis results is shown in Fig. 14b for the L'Aquila seismic record. As expected, the safe domain narrows down with a reduced intensity earthquake: for the record scaled by 50%, the masonry block always survives, whereas for the unscaled record the collapse domain is for 0< <0.8. The block with smaller thickness (0.16 m, case #1) is less stable than the block with larger thickness (0.20 m, case #2) for almost all cases (Fig. 14c-f). Furthermore, the free-standing masonry block shows higher normalized rotations than the block with the roof mass. Larger roof mass generally corresponds to lower normalized rotations, so the scale effect related to the block shape prevails (Fig. 14c-d). If the horizontal thrust of 50 N/m is considered, the blocks with =0 and =1.0 overturn for both cases #3 and #4. For the same record, a thrust of 100 N/m causes the block to overturn for all values of . The latter result is valid also for CMEND record, the one with the highest PGV. The added mass has a positive stabilizing effect, but the previously discussed scale effect does not appear. As a matter of fact, the maximum normalized rotations are nearly constant for the case #3 (H=0 and H=50 N/m) and for the case #4 (H=0). It should be noticed that, whenever the masonry block survives the earthquake, the maximum response over motion is nearly constant for different values (Fig. 14 from a to d) when no thrust is applied. The roof thrust strongly influences the response also for the acceleration time-histories with smaller PGV and PGA, namely FRIU and MOG (Fig. 14e-f). For this reason, the presence of the outward thrust has to be accurately considered with a proper safety factor. Values of distributed loads on the roof p_r higher than those assumed, with no thrust, cause maximum normalized rotations sensitively lower than those displayed in Fig. 14 (from c to f).

6.3 Kinematic analysis

A non-linear kinematic analysis was also carried out to compare it with the results of the rocking analysis. The varied parameter is still β and the verification was performed in terms of ultimate limit state attained. If the ultimate limit state is attained, namely the capacity is lower than the displacement demand, the collapse is considered to occur. The displacement response spectra are those obtained from the recorded earthquakes (Table 2). When neither additional mass nor horizontal thrust is considered, the displacement capacity is basically the same if β changes (namely, the block shape changes) and the thickness remains constant. This is due to the non-linear kinematic curve, and in particular the acceleration triggering motion, being mainly influenced by the thickness of the wall rather than by the angle β. Indeed, the angle only slightly affects the radius vector which, for example, varies from 1 m for β =0 to 1.26 m for β =1 rad in the case of 0.20m thick masonry blocks.

When an additional roof weight is considered at the top of the wall panel, the displacement capacity decreases with respect to the free-standing block. It means that the destabilizing out-of-plane effect prevails on the stabilizing effect provided by the increased mass. In all the kinematic analyses, the ultimate limit state is attained for all β values and for all cases specified in Table 3, with some exceptions. Indeed, for cases #2, #3a and#4a the capacity is

lower than the demand respectively in 93%, 87% and 97% of the analyses, all related to the Friuli seismic record.

6.4 Comparison between rocking and kinematic analysis

In the rocking analysis, one can notice that the block performance is affected by the choice of the β values. By contrast, in the kinematic analysis this strong dependency has not been found. For the free-standing block, the kinematic approach nearly provides the same displacement capacity for all values. However, the most critical β value cannot be defined *a priori* in either procedures. The rocking analysis should be carried out not only for one or two values, but for a few values, since non-conservative responses can be filtered. The effect of an added roof mass can be either negative or positive in the kinematic analyses, whereas in the rocking analysis is generally stabilizing. Furthermore, in the rocking analysis, the response strongly depends on the type of seismic record. In the rocking analysis, collapse occurs in 47% of the cases with Friuli seismic record (from Fig. 14f), while in the kinematic analysis the collapse occurs on average in 93% of the cases. Once again, the kinematic approach is found to be over-conservative with respect to the dynamic analysis, and therefore may often lead to expensive and sometimes unnecessary retrofitting measures, particularly negative for historical buildings.

7 CONCLUSIONS

This paper investigates the rocking response of masonry walls connected to roofs. Many collapses of masonry portions supporting roofs occurred in the last Italian earthquakes, probably due to the roof thrust that acted with destabilizing effect. The Housner's equation of motion of the free-standing SDOF block has been modified by considering the possible roof mass and the roof thrust.

The dependence of the restoring moment on the rotation ϑ was studied and the minimum horizontal stiffness K_{min} needed to obtain the same ultimate displacement as the system without thrust, was calculated. This value depends on the roof thrust, on the radius vector and on the slenderness ratio. A parametric analysis showed a scale effect for which larger masonry blocks with the same slenderness can more easily survive earthquakes due to their higher rotational inertia, so requiring a lower minimum stiffness K_{min}.

Two case studies, the dynamics of which is evaluated with a purposely developed MATLAB code, were presented as practical application. The first one regards an URM structure tested on shaking table. A vulnerability assessment was carried out by applying the non-linear kinematic approach suggested by the Italian code for out-of-plane mechanisms. Unlike the code procedure which assessed an unsafe condition for a PGA=0.25g, the rocking block subjected to the same incremental acceleration time-history as the experimental one collapsed at PGA=0.5 g, confirming the experimental results. The second case study is a trapezoidal spandrel beam subjected to a roof thrust, which survived during the Emilia Romagna earthquake in 2012. The spandrel beam survived the two acceleration time-histories recorded at the epicenter without collapse, only exhibiting small rotation values over the entire motion. In both cases, the damping effects were considered in the Housner's formulation in terms of theoretical value of restitution coefficient. Conversely, also in this case the kinematic analysis would have predicted a failure of the block.

Inertia moments and radius vectors of different types of failure mechanisms have been provided to allow the user to solve the SDOF motion equation for different block shapes. In particular, the trapezoidal block, a very frequent shape in masonry façades due to the influential effect of openings, together with the corner mechanism, were considered. For the corner mechanism, the full moment of inertia tensor was provided, as well as the scalar moment of inertia about an axis of rotation generically oriented in the space. For the trapezoidal block, a parametric analysis was carried out by changing its geometrical shape; it was highlighted the dependency of the dynamic performance on the block shape, and the need of considering a number of different shapes to ensure a conservative numerical prediction. The collapse of the rocking block was found to be more likely for seismic records with higher PGV. A corresponding kinematic analysis has been carried out; once again the kinematic approach was found to be overly conservative with respect to the dynamic analysis. The use of the rocking analysis can therefore be crucial for historic buildings, where too conservative results could lead to unnecessary and expensive retrofitting measures.

The main findings of this paper can be summarized as follows.
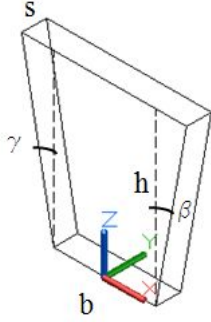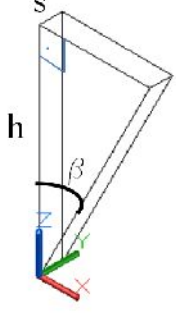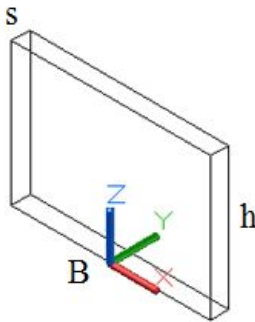
1. The additional roof mass generally causes lower normalized rotations with respect to the case of no roof mass, due to the fact that the radius vector of the entire block + roof system mass is larger than that of the masonry block alone.

2. The roof thrust, if any, must be taken into account, due to its strong influence on the wall response. Even small thrust values can cause the sudden collapse of the block; it is therefore recommended that the roof thrust is always multiplied by an appropriate safety factor.

3. When a vulnerability assessment of a spandrel beam below a roof has to be made, a parametric analysis should be performed by varying the block shape, since this parameter could markedly affect the dynamic response of the block.

4. In the case of trapezoidal masonry blocks, frequent in current practice, kinematic analysis led to overly conservative results with respect to rocking analysis.

APPENDIX A. MOMENTS OF INERTIA AND RADIUS VECTORS FOR DIFFERENT BLOCK SHAPES

Several failure mechanisms can occur in the out-of-plane response of masonry walls. These failure mechanisms can concern simple rectangular, triangular or trapezoidal blocks (Fig. 15). The latter ones, where each side edge is inclined of an angle β and γ with respect to the vertical, depend on the location of openings in the façade.

Openings are indeed weak points: their geometry and position with respect to the corners of the building influence the shape of possible out-of-plane mechanisms. The values of the length of the semi-diagonal R and of the inertia moment I_0 (which does not take into account the possible added roof mass) are necessary to solve the motion equation and obtain the rocking response under a given acceleration time-history. Fig. 15 summarizes the formulas to calculate R and I_0 for different block shapes having specific density ρ. The axes are denoted with X along the block length, Z in vertical direction and Y along the wall thickness. The inertia moment of the triangular block is necessary for the calculation of the inertia moments of the corner mechanism, which is presented later.

The rocking rotation is assumed to occur at the axes origin. Nevertheless, to consider a finite compressive strength of masonry, one could modify the total thickness s of the wall by subtracting the quantity $u = 2N/(3\bar{b}f_m)$, where N denotes the self weight of the block, $\bar{b}$ signifies the (variable) base width, and f_m denotes the compressive masonry strength. This latter expression is obtained by assuming a triangular stress block, and a rocking rotation about the point at 1/3rd of the stress block from its compressed side.

Block shape			
R	$\sqrt{\left[\dfrac{1}{3}\dfrac{3bh + 2h^2(\tan\beta + \tan\gamma)}{2b + h(\tan\beta + \tan\gamma)}\right]^2 + \dfrac{s^2}{4}}$	$\sqrt{\dfrac{h^2}{9}(4 + \tan^2\beta) + \dfrac{s^2}{4}}$	$\dfrac{\sqrt{h^2 + s^2}}{2}$
$I_{0,XX}$	$\rho sh\left[\dfrac{h}{2}(\tan\beta + \tan\gamma)\left(\dfrac{h^2}{2} + \dfrac{s^2}{3}\right) + \dfrac{b}{3}(h^2 + s^2)\right]$	$\rho s\dfrac{h^2}{2}\tan\beta\left(\dfrac{h^2}{2} + \dfrac{s^2}{3}\right)$	$\dfrac{\rho sBh}{3}(h^2 + s^2)$

Fig. 15. Radius vectors, R, and axial inertia moments, $I_{0,XX}$, about the rotation axis X, of different block shapes. ρ denotes the specific density.

By composing the moments of inertia of the 3D blocks displayed in Fig. 15, it is possible to write the moment of inertia tensor of the corner of a building, like in Fig. 16a. For a simpler calculation, the corner has been assumed to be made of two triangular blocks of thickness s_1, s_2 and shape defined by the angles   and   respectively (Fig. 16b). First, the moment of inertia tensor $\mathbf{I}$ of the building corner with respect to the axes X, Y, Z (Fig. 16b) at the lower plastic hinge is calculated. Secondly, a generic rotation axis $\vec{\omega}$ can be defined by $\vec{\omega} = \omega\vec{n}$, where $\vec{n}^T = (\cos\delta_X \cos\delta_Y \cos\delta_Z)$ are the direction cosines with respect to the initial axes. It is then possible to calculate the scalar moment of inertia I with respect to the axis of rotation $\vec{\omega}$ with the simple matrix multiplication:
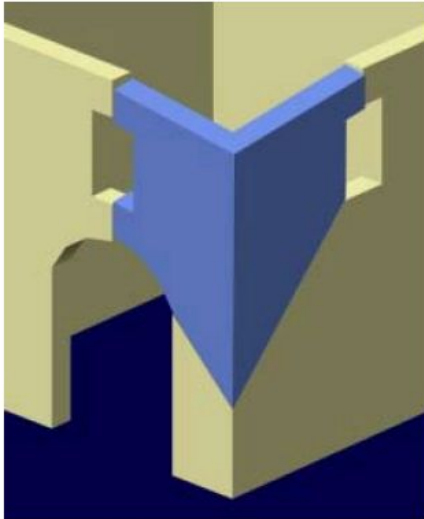
$$I = \vec{n}^T \mathbf{I}\vec{n} \tag{24}$$

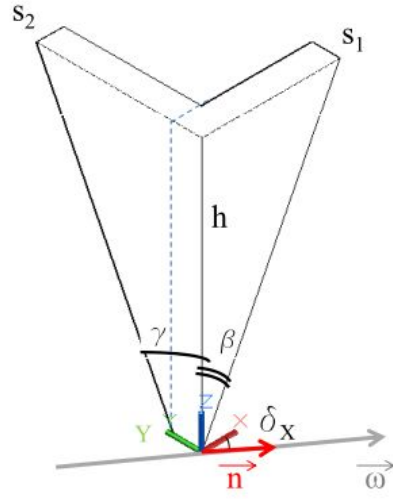The moment of inertia tensor of the rigid corner block displayed in Fig. 166b is:

$$I = \rho h^2 \begin{bmatrix} \left[\begin{array}{l} \frac{s_1}{2}\tan\beta\left(\frac{h^2}{2}+\frac{s_1^2}{3}\right)+ \\ +s_2\frac{h^2}{4}\tan\gamma\left(1+\frac{\tan^2\gamma}{3}\right)+ \\ +\frac{s_1^2 s_2}{2}\tan\gamma+\frac{s_1 s_2 h}{3}\tan^2\gamma+ \end{array}\right] & -\frac{1}{4}\left[\begin{array}{l} s_1^2\frac{h}{3}\tan^2\beta+ \\ +s_2^2\tan\gamma\left(s_1+\frac{h}{3}\tan\gamma\right) \end{array}\right] & -\frac{1}{2}\left[\begin{array}{l} s_1\frac{h^2}{4}\tan^2\beta+ \\ s_2^2\frac{h}{3}\tan\gamma \end{array}\right] \\[3em] -\frac{1}{4}\left[\begin{array}{l} s_1^2\frac{h}{3}\tan^2\beta+ \\ +s_2^2\tan\gamma\left(s_1+\frac{h}{3}\tan\gamma\right) \end{array}\right] & \frac{1}{2}\left[\begin{array}{l} s_1\frac{h^2}{2}\tan\beta\left(1+\frac{\tan^2\beta}{4}\right)+ \\ +\frac{s_1 h^2}{24}\tan^3\beta+ \\ +s_2\tan\gamma\left(\frac{h^2}{2}+\frac{s_2^2}{3}\right) \end{array}\right] & -h\left[\begin{array}{l} \frac{s_1^2}{6}\tan\beta+s_2\frac{h}{8}\tan^2\gamma+ \\ +\frac{s_1 s_2}{3}\tan\gamma \end{array}\right] \\[3em] -\frac{1}{2}\left[\begin{array}{l} s_1\frac{h^2}{2}\tan^2\beta+ \\ s_2^2\frac{h}{3}\tan\gamma \end{array}\right] & -h\left[\begin{array}{l} \frac{s_1^2}{6}\tan\beta+s_2\frac{h}{8}\tan^2\gamma+ \\ +\frac{s_1 s_2}{3}\tan\gamma \end{array}\right] & \frac{1}{6}\left[\begin{array}{l} \frac{h^2}{2}(s_1\tan^3\beta+s_2\tan^3\gamma)+ \\ +s_1^3\tan\beta+s_2^3\tan\gamma+ \\ +\frac{6}{h}s_1 s_2\tan\gamma\left(s_1\frac{h}{2}+\frac{h^2}{3}\tan\gamma\right) \end{array}\right] \end{bmatrix} \tag{25}$$

while the radius vector R with respect to the main axes reads:

$$R = \begin{bmatrix} R_X \\ R_Y \\ R_Z \end{bmatrix} = \begin{bmatrix} \dfrac{\frac{s_1 h\tan^2\beta}{3}+\frac{s_2^2\tan\gamma}{2}}{s_1\tan\beta+s_2\tan\gamma} \\[1.5em] \dfrac{s_1^2\tan\beta+2s_2\tan\gamma\left(\frac{h}{3}\tan\gamma+s_1\right)}{2(s_1\tan\beta+s_2\tan\gamma)} \\[1.5em] \dfrac{2}{3}h \end{bmatrix} \tag{26}$$

Fig. 16. (a) Corner failure mechanism [30] and (b) geometry of the block.

The moment of inertia tensor I and the radius vector R can be simplified if the thicknesses s_1, s_2 are the same and equal to s, and $\beta = \gamma$:

$$I = \rho s h^2 \begin{bmatrix} \tan\beta \begin{bmatrix} \frac{h^2}{4}\left(2 + \frac{\tan^2\beta}{3}\right) + \\ + \frac{2}{3}s^2 + \frac{1}{3}sh\tan\beta \end{bmatrix} & -\frac{\tan\beta}{2}\left(\frac{h}{3}\tan\beta + \frac{s}{2}\right) & -\frac{h}{2}\tan\beta\left(\frac{h}{4}\tan\beta + \frac{s}{3}\right) \\ -\frac{\tan\beta}{2}\left(\frac{h}{3}\tan\beta + \frac{s}{2}\right) & \frac{\tan\beta}{2}\left[\frac{h^2}{2}\left(2 + \frac{\tan^2\beta}{3}\right) + \frac{s^2}{3}\right] & -\frac{h}{2}\tan\beta\left(\frac{h}{4}\tan\beta + s\right) \\ -\frac{h}{2}\tan\beta\left(\frac{h}{4}\tan\beta + \frac{s}{3}\right) & -\frac{h}{2}\tan\beta\left(\frac{h}{4}\tan\beta + s\right) & \frac{\tan\beta}{3}\left[\frac{h^2}{2}\tan^2\beta + sh\tan\beta + \frac{5s^2}{2}\right] \end{bmatrix} \quad (27)$$

$$R = \begin{bmatrix} R_X \\ R_Y \\ R_Z \end{bmatrix} = \begin{bmatrix} \frac{1}{2}\left(\frac{h}{3}\tan\beta + \frac{s}{2}\right) \\ \frac{1}{2}\left(\frac{h}{3}\tan\beta + \frac{3s}{2}\right) \\ \frac{2}{3}h \end{bmatrix} \quad (28)$$

The tensors and vectors given by Equations (25) to (28) are useful to study the dynamics of the corner mechanism about a generic axis of rotation. For example, if the axis of rotation is at 45° with respect to the X axis and lays in the plane X-Y, the unit vector is $\vec{n}^T = (\cos\delta_X \cos\delta_Y \cos\delta_Z) = \frac{\sqrt{2}}{2}(1 \ -1 \ 0)$. Therefore, from Equation (24) one has:

$$\hat{I} = I_{XX}\cos^2\delta_X + I_{YY}\cos^2\delta_Y + 2I_{XY}\cos\delta_X\cos\delta_Y = \frac{1}{2}(I_{XX} + I_{YY}) - I_{XY} \quad (29)$$

where the terms I_{XX}, I_{YY} and I_{XY} of the moment of inertia tensor are provided by the tensor in Equation (25) for the general case and in Equation (27) for the symmetric case $s_1 = s_2$ and $\beta = \gamma$. The rotation axis should be varied to take into account different moments of inertia, which could affect the dynamic response of the corner block.

Acknowledgements

REFERENCES

[1] Giuffrè A. Seismic damage in historic town centers and attenuation criteria. Ann Geofis 1995;38:837–43.

[2] Casolo S, Uva G. Nonlinear analysis of out-of-plane masonry façades: full dynamic versus pushover methods by rigid body and spring model. Earthquake Engng Struct. Dyn. 2013;42:499–521.

[3] Lagomarsino S. A new methodology for the post-earthquake investigation of ancient churches. Proc. of the 11th European Conference on Earthquake Engineering 1998:67.

[4] D'Ayala D, Speranza E. Definition of Collapse Mechanisms and Seismic Vulnerability of Historic Masonry Buildings. Earthquake Spectra 2003;19:479–509.

[5] Giresini L. Modelling techniques and rocking analysis for historic structures: influence of vaulted systems in the seismic response of churches. PhD. thesis, University of Pisa; 2014.

[6] Housner GW. The behavior of inverted pendulum structures during earthquakes. Bulletin of the Seismological Society of America 1963;53:403–17.

[7] Nuove Norme Tecniche per le Costruzioni, D.M. 14/01/2008, approvazione delle nuove norme tecniche per le costruzioni, G. U. della Repubblica Italiana, n. 29 del 4 febbraio 2008 Supplemento Ordinario n. 30; 2008 (In Italian).

[8] Circolare esplicativa del 02.02.2009 contenente "Istruzioni per l'applicazione delle nuove norme tecniche per le costruzioni di cui al D.M. 14.01.2008" (In Italian).

[9] Giresini L, Fragiacomo M, Lourenço PB. Comparison between rocking analysis and kinematic analysis for the dynamic out-of-plane behavior of masonry walls. Earthquake Engineering and Structural Dynamics 2015.

[10] De Falco A, Giresini L, Sassu M. Temporary preventive seismic reinforcements on historic churches: numerical modeling of San Frediano in Pisa. Applied Mechanics and Materials 2013;351-352:1393–6.

[11] Giresini L, Sassu M. Guidelines for designing temporary preventive anti-seismic safety features for historic churches, ReLUIS 2013; 2013.

[12] Andreini M, De Falco A, Giresini L, Sassu M. Collapse of the historic city walls of Pistoia (Italy): causes and possible interventions. Applied Mechanics and Materials 2013;352:1389–92.

[13] Giuffrè A. Sicurezza e conservazione dei centri storici. Il caso Ortigia: Laterza; 1993.

[14] Makris N. The Role of the Rotational Inertia on the Seismic Resistance of Free-Standing Rocking Columns and Articulated Frames. Bulletin of the Seismological Society of America 2014;104:2226–39.

[15] Makris N, Zhang J. Rocking Response of Anchored Blocks under Pulse-Type Motions. Journal of Engineering Mechanics 2001;127:484–93.

[16] Makris N, Vassiliou MF. Dynamics of the Rocking Frame with Vertical Restrainers. J. Struct. Eng. 2014:4014245.

[17] Al Shawa O, de Felice G, Mauro A, Sorrentino L. Out-of-plane seismic behaviour of rocking masonry walls. Earthquake Engng Struct. Dyn. 2012;41:949–68.

[18] Sorrentino L, AlShawa O, Decanini LD. The relevance of energy damping in unreinforced masonry rocking mechanisms. Experimental and analytic investigations. Bulletin of Earthquake Engineering 2011;9:1–26.

[19] Sorrentino L, Liberatore L, Liberatore D, Masiani R. The behaviour of vernacular buildings in the 2012 Emilia earthquakes. Bulletin of Earthquake Engineering 2014;12:2367–82.

[20] Chapra SC, Canale RP. Numerical Methods for Engineers; 2010.

[21] Dolce M, Ponzo FC, Di Croce M, Moroni C, Giordano F, Nigro D. et al. Experimental assessment of the CAM and DIS-CAM systems for the seismic upgrading of monumental masonry buildings. Proceeding of 1st international conference on protection of historical constructions, Roma, Italy 2009:1021–7.

[22] De Canio G de, Dolce M, Goretti A, Marnetto R. Progetto TREMA–Tecnologie per la Riduzione degli Effetti sismici sui Manufatti Architettonici in muratura e in c.a.: MURST Legge n. 449/1997, D.M. 10 Maggio 2000 (in Italian).

[23] Betti M, Galano L, Vignoli A. Comparative Analysis on the Seismic Behaviour of Unreinforced Masonry Buildings with Flexible Diaphragms. Engineering Structures 2014;61:195–208.

[24] Sorrentino L, Kunnath S, Monti G, Scalora G. Seismically induced one-sided rocking response of unreinforced masonry façades. Engineering Structures 2008;30:2140–53.

[25] FEMA 356. Prestandard and Commentary for the Seismic Rehabilitation of Buildings.

[26] Makris N, Kostantinidis D. The rocking spectrum and the limitations of practical design methodologies. Earthquake Engineering and Structural Dynamics 2003;32:265–89.

[27] Makris N, Roussos Y. Rocking response of rigid blocks under near-source ground motions. Geotechnique 2000;50:243–62.

[28]   Accelerograms Database of seismic shocks on May, 29th2012, Emilia Romagna region (Italy). Department of Italian Civil Protection; 2012; Available from: http://www.mot1.it/randownload/EN/index.php.

[29]   http://peer.berkeley.edu/smcat/data.html. Peer Strong Motion Database Record Processed By Pacific Engineering; 2014.

[30]   Beolchini GC, Milano L, Antonacci E. Repertorio dei meccanismi di danno, delle tecniche di intervento e dei relativi costi negli edifici in muratura: Analisi dei Meccanismi Locali in Edifici Esistenti in Muratura. L'Aquila; 2006.